

NASA/TM-20220010894



Acoustic Modeling of Novel Over-the-Rotor Acoustic Liner Concepts Using COMSOL Multiphysics® Simulation Software

Alexander Svetgoff
Glenn Research Center, Cleveland, Ohio

NASA STI Program . . . in Profile

Since its founding, NASA has been dedicated to the advancement of aeronautics and space science. The NASA Scientific and Technical Information (STI) Program plays a key part in helping NASA maintain this important role.

The NASA STI Program operates under the auspices of the Agency Chief Information Officer. It collects, organizes, provides for archiving, and disseminates NASA's STI. The NASA STI Program provides access to the NASA Technical Report Server—Registered (NTRS Reg) and NASA Technical Report Server—Public (NTRS) thus providing one of the largest collections of aeronautical and space science STI in the world. Results are published in both non-NASA channels and by NASA in the NASA STI Report Series, which includes the following report types:

- TECHNICAL PUBLICATION. Reports of completed research or a major significant phase of research that present the results of NASA programs and include extensive data or theoretical analysis. Includes compilations of significant scientific and technical data and information deemed to be of continuing reference value. NASA counter-part of peer-reviewed formal professional papers, but has less stringent limitations on manuscript length and extent of graphic presentations.
- TECHNICAL MEMORANDUM. Scientific and technical findings that are preliminary or of specialized interest, e.g., “quick-release” reports, working papers, and bibliographies that contain minimal annotation. Does not contain extensive analysis.
- CONTRACTOR REPORT. Scientific and technical findings by NASA-sponsored contractors and grantees.
- CONFERENCE PUBLICATION. Collected papers from scientific and technical conferences, symposia, seminars, or other meetings sponsored or co-sponsored by NASA.
- SPECIAL PUBLICATION. Scientific, technical, or historical information from NASA programs, projects, and missions, often concerned with subjects having substantial public interest.
- TECHNICAL TRANSLATION. English-language translations of foreign scientific and technical material pertinent to NASA's mission.

For more information about the NASA STI program, see the following:

- Access the NASA STI program home page at <http://www.sti.nasa.gov>
- E-mail your question to help@sti.nasa.gov
- Fax your question to the NASA STI Information Desk at 757-864-6500
- Telephone the NASA STI Information Desk at 757-864-9658
- Write to:
NASA STI Program
Mail Stop 148
NASA Langley Research Center
Hampton, VA 23681-2199

NASA/TM-20220010894



Acoustic Modeling of Novel Over-the-Rotor Acoustic Liner Concepts Using COMSOL Multiphysics[®] Simulation Software

Alexander Svetgoff
Glenn Research Center, Cleveland, Ohio

National Aeronautics and
Space Administration

Glenn Research Center
Cleveland, Ohio 44135

December 2022

This work was sponsored by the Advanced Air Vehicle Program
at the NASA Glenn Research Center

Trade names and trademarks are used in this report for identification
only. Their usage does not constitute an official endorsement,
either expressed or implied, by the National Aeronautics and
Space Administration.

Level of Review: This material has been technically reviewed by technical management.

Acoustic Modeling of Novel Over-the-Rotor Acoustic Liner Concepts Using COMSOL Multiphysics® Simulation Software

Alexander Svetgoff
National Aeronautics and Space Administration
Glenn Research Center
Cleveland, Ohio 44135

Summary

This report presents simulation predictions of novel over-the-rotor (OTR) acoustic liner configurations compared with experimental data. This is a follow-on to an investigation on the effect of grazing flow on grooved OTR casing treatments, which determined that traditional liner modeling techniques are inadequate for nontraditional internal liner cavity geometries. A series of these expansion-chamber-type liner design concepts were previously developed by the NASA Glenn Research Center and tested using the NASA Langley Research Center Normal Incidence Tube. In this investigation, the measured normalized impedance and absorption coefficient were compared with those obtained from a COMSOL Multiphysics® (COMSOL AB) software simulation. Additionally, using a parametric case study, another series of simulations were conducted to determine what additional benefits, if any, this type of liner has to offer the acoustics community. In total, 53 permutations of this concept were investigated. The results indicate that with longer internal fins, the resonance is shifted to lower frequencies.

1.0 Introduction

Analysis and development of aircraft noise reduction technology has been part of NASA's projects for decades. One of the main contributors to the overall noise signature of a modern subsonic aircraft is fan noise. Traditional passive acoustic liner concepts are accurately modeled using the Zwikker–Kosten Transmission Line (ZKTL) model (Refs. 1 and 2), but the newer classes of subsonic turbofan aircraft engines yield less volume in the confines of the nacelle for acoustic casing treatments. Because traditional honeycomb-over-perforate liners are not well suited for use in this environment, many other liner concepts, such as metallic foams, have been explored (Refs. 3 and 4). Over the last decade or so, NASA has been investigating the efficacy of placing acoustic treatment over the rotor (OTR) to reduce the overall noise signature of modern aircraft engines (Refs. 5 to 15). Recognizing that the nature of the acoustic field somewhat resembles the shock wave, Bozak (Refs. 4 and 6) imagined a novel expansion-chamber-type geometry design. A schematic of the expansion chamber design concept is shown in Figure 1.

Due to the design's more complex interior geometry, the traditional ZKTL modeling technique was deemed inadequate for predicting the acoustic response. This is exemplified in Figure 2, which compares the ZKTL prediction for an expansion chamber design with the experimental results. In general, the ZKTL prediction fails to capture the expansion chamber design's complex interior geometry. The effects of certain interior characteristics, such as expansion chamber fin angle, are not captured with the ZKTL method.

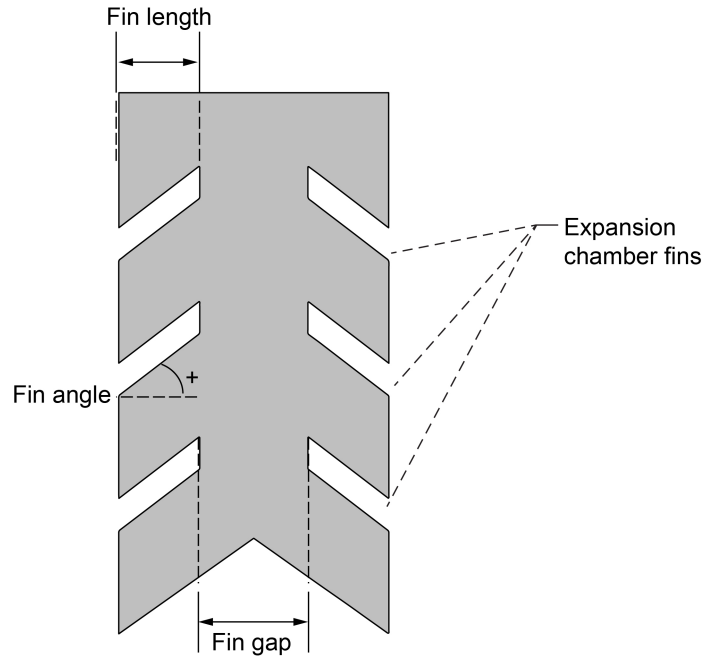


Figure 1.—Expansion chamber design concept.

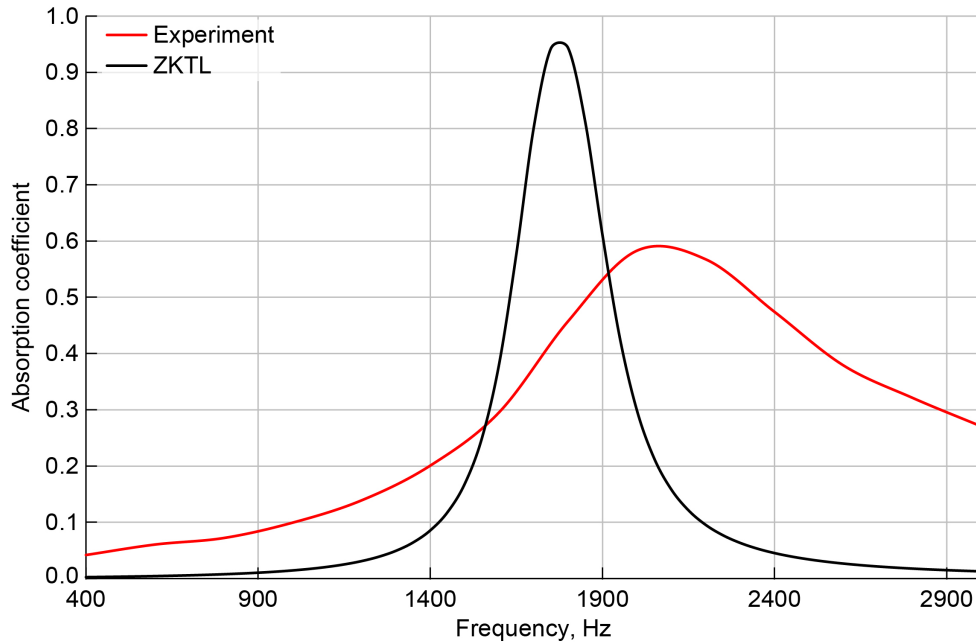


Figure 2.—Simple Zwikker–Kosten Transmission Line (ZKTL) prediction for expansion chamber geometry concept compared with experimental test case.

The OTR expansion chamber geometry concept was first realized by Bozak and tested at the Langley Research Center (Refs. 4, 6, 14, and 16). A series of 25 different configurations were tested using the Langley Normal Incidence Tube (NIT). First, these liner prototypes were manufactured using three-dimensional (3D) printers to analyze their overall suitability as a liner concept. Next, the best performing

concept was tested under grazing flow using the Langley Grazing Flow Impedance Tube (GFIT). Due to the concept liner's more complex interior geometry, ZKTL was deemed inadequate to predict the acoustic response. Instead, COMSOL Multiphysics® (COMSOL AB) was selected to perform the simulations with the objective of accurately capturing the acoustic response regardless of the interior geometry.

The normalized impedance and absorption coefficient for numerous OTR expansion chamber geometries were modeled and compared with the measured results (Ref. 17) using the pressure acoustics physics module in COMSOL Multiphysics®. During this investigation, the COMSOL Multiphysics® built-in perforate model was analyzed for its viability against other perforate models used in the acoustics industry and will be discussed in a later section.

2.0 Simulation Methods

2.1 Model Setup

The simulation was set up to mimic the NIT, which incorporates the ASTM E1050–12 standard for measuring the impedance using the two-microphone method (Refs. 18 and 19). The model incorporated the 2.0- by 2.0-in. waveguide, two measurement microphones at 2.50 and 3.75 in., and a reference microphone at 0.25 in. (microphone distances are measured from liner surface). The sound source was generated using an overall sound pressure level plane-wave excitation of 120 dB from a frequency range of 400 to 3000 Hz. The cavity surfaces were modeled with an impedance boundary condition. Figure 3 shows the NIT compared with the COMSOL Multiphysics® model.

The pressure acoustics interface was used to model the acoustic field and was discretized using quadratic Lagrange elements. Using this type of discretization allows for the acoustic wave to be resolved with a minimum of five elements per wavelength. For each of the cases presented in this report, more than five elements per wavelength were used. The mesh comprised a swept grid for the components of the modeled impedance tube above the lowest microphone plane, and an unstructured tetrahedral grid was used everywhere else.

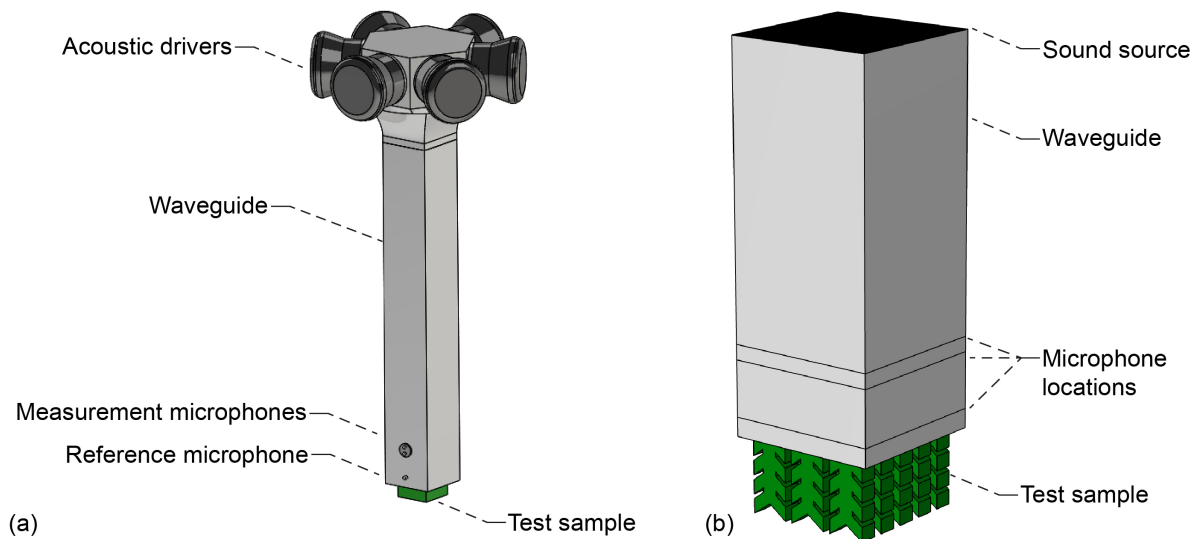


Figure 3.—Comparison of NASA Langley Research Center Normal Incidence Tube (NIT) with COMSOL Multiphysics® model. (a) NIT. (b) COMSOL Multiphysics® simulation of NIT.

2.2 Facesheet Models

The transfer impedance is defined by the ratio of the pressure drop across the facesheet relative to the normal particle velocity at the surface of the facesheet. For the no-flow test case, four different facesheet models were analyzed: a wave propagation model (WPM), a two-parameter model (TPM), the COMSOL Multiphysics[®] analytical transfer impedance model (ATIM), and the COMSOL Multiphysics[®] simulated transfer impedance model (STIM) (Refs. 20 to 22). The WPM (also implemented in ZKTL) only considered the linear effects of the direct-current (DC) flow resistance for the facesheet and used Melling's model to compute the mass reactance. The TPM separated the DC flow resistance into linear and nonlinear contributions, and the mass reactance contained portions to evaluate with and without the presence of flow. The COMSOL Multiphysics[®] ATIM was a semi-analytical model that used Crandall's model for the linear DC flow resistance and then Melling's model for the mass reactance. The COMSOL Multiphysics[®] STIM used the thermoviscous acoustics interface to account for the linear losses due to the perforate as well as the hole-to-hole interaction effects that accompany the thermal and viscous losses. The facesheet perforate properties for all of the test cases had a porosity of 10 percent, a perforate thickness of 0.06 in., and a perforate hole diameter of 0.035 in.

2.3 Facesheet Model Results

The real and imaginary parts of the transfer impedance were compared for each of the acoustic models. The WPM was executed using a MATLAB[®] (The MathWorks, Inc.) code, the TPM was implemented directly in COMSOL Multiphysics[®], the COMSOL Multiphysics[®] ATIM used the built-in perforate model, and the COMSOL Multiphysics[®] STIM used a separate physics node in the software to do the comprehensive simulation. Figure 4 is a comparison of each model.

It is clear that each of the models produces a different real part of the transfer impedance. In the case of the imaginary part, the WPM and the COMSOL Multiphysics[®] analytical model lie on top of one another. This is expected, because both incorporated Melling's model to compute the mass reactance. The problem with this comparison is the uncertainty as to which model is most accurate for the problem at hand. In an attempt to alleviate this uncertainty, the models were coupled with the liner in question and then compared with the experiment. Once the transfer impedance was known for COMSOL Multiphysics[®] STIM, that transfer impedance was used as a boundary condition for the full liner model. Figure 5 shows the effect of incorporating the transfer impedance at the boundary condition on all of the liner cavity surfaces.

Starting with Figure 5(a), all of the models except the TPM align with the experimental normalized resistance reasonably well between 1000 and 2000 Hz. In Figure 5(b), the TPM prediction crosses paths with the experiment, whereas the other models evaluated fall slightly below the experiment and the TPM prediction. Similar to Figure 5(b), Figure 5(c) illustrates that, with the exception of the TPM, each of the prediction models misses the absorption peak by about 250 Hz. Regarding Figure 5(a), a brief discussion may be necessary as to why the experimentally measured normalized resistance diverges near the data set bounds. A study by Jones and Watson (Ref. 23) attributes the divergence seen in the experimental data set near the data set bounds to viscothermal effects from the walls of the cavities and does not consider it an artifact resulting from nonlinearities in the facesheet. The diverging effects are not captured in the physics-based model because the thermoviscous acoustics interface is very computationally expensive for a problem of this size. Nonetheless, it is clear that the TPM prediction matches best with the experimentally deduced absorption coefficient.

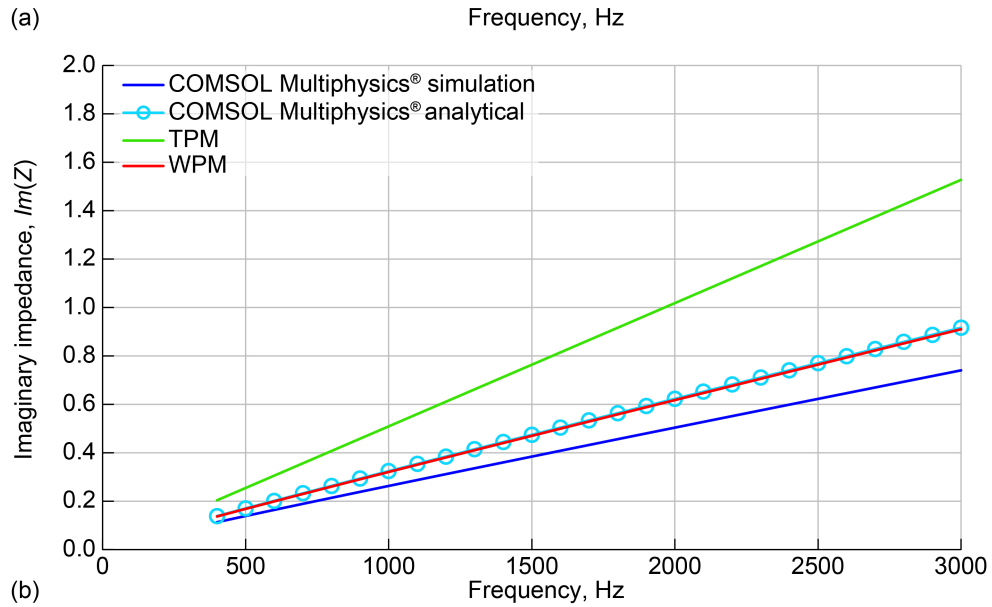
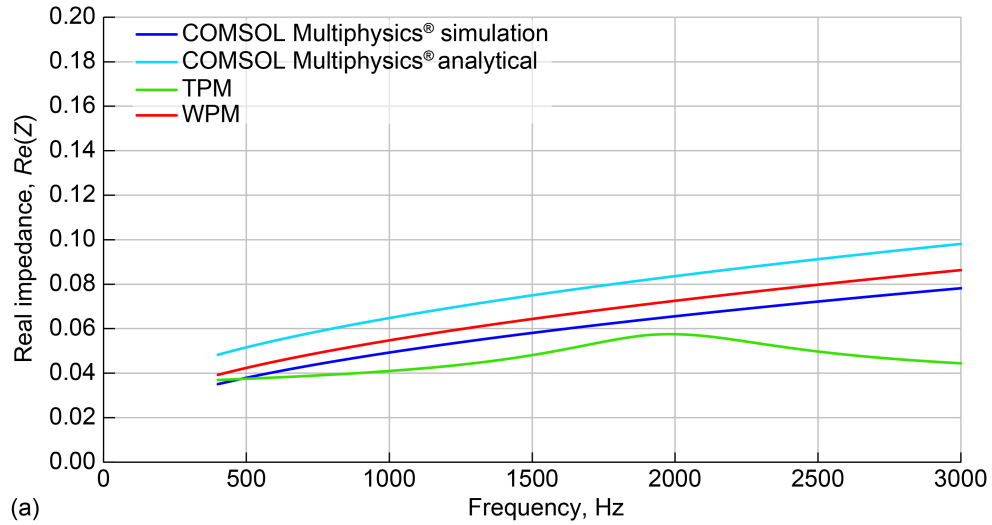


Figure 4.—Comparison of parts of perforate transfer impedance for each acoustic model. Two-parameter model, TPM; wave propagation model, WPM. (a) Real impedance, $Re(Z)$. (b) Imaginary impedance, $Im(Z)$.

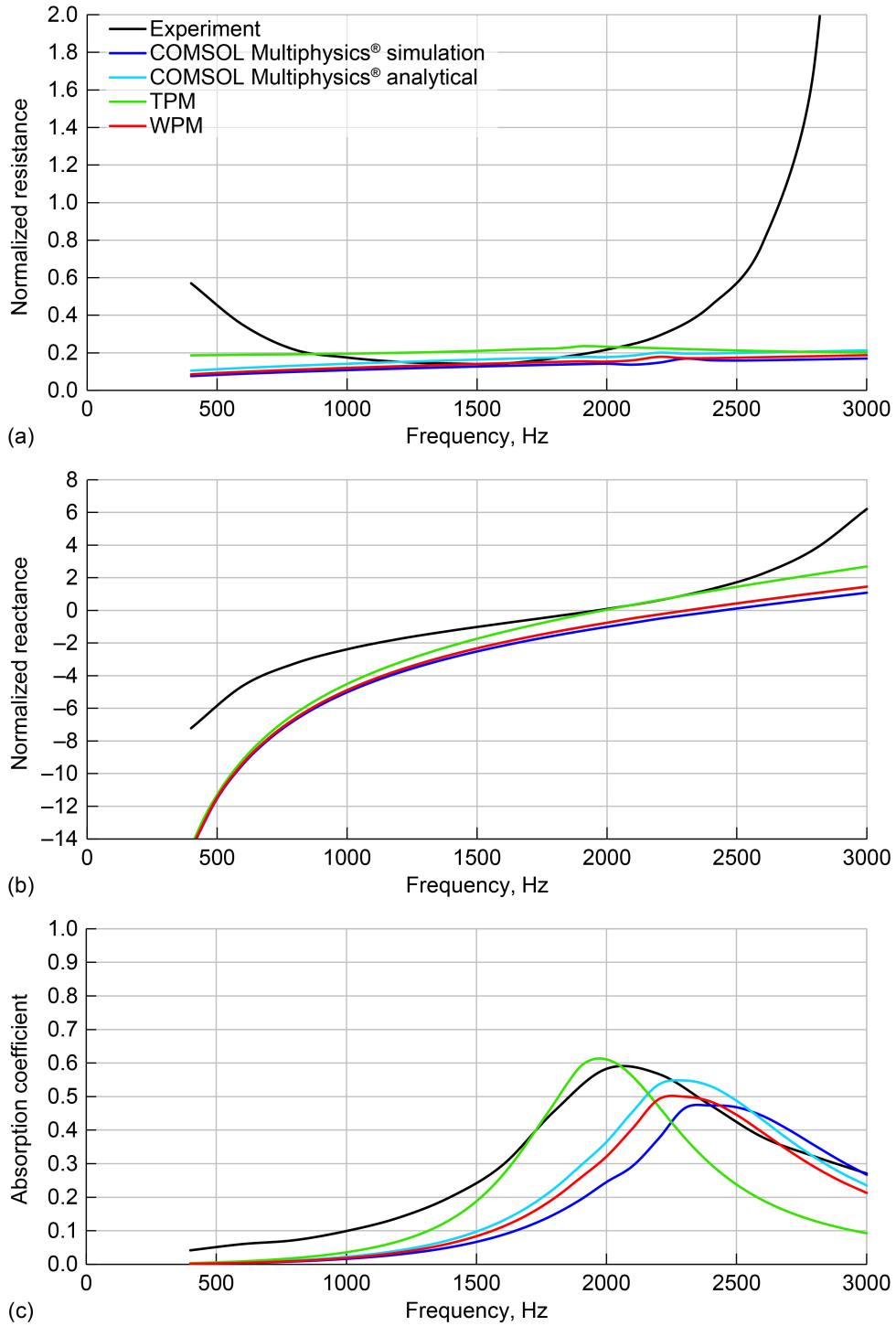


Figure 5.—Comparison of acoustic properties for transfer impedance applied to liner cavity surfaces. (a) Normalized resistance. (b) Normalized reactance. (c) Absorption coefficient.

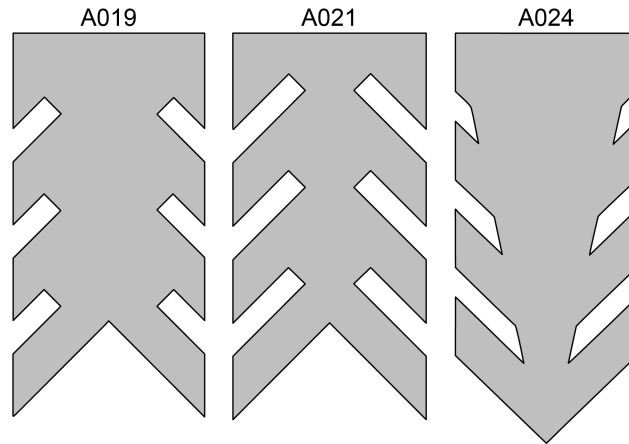


Figure 6.—Expansion chamber geometries modeled using COMSOL Multiphysics®.

The TPM model is also reliant on liner cavity geometry being present to accurately predict the impedance. The TPM model required an iterative process to converge on the root-mean-square (RMS) particle velocity and impedance at the facesheet surface. Because these simulations run very quickly, it is easy to converge in roughly three to four runs by linearly modifying the RMS particle velocity by 10 percent for each run. At this point, the difference between the last two runs is negligible (about 0.02 percent).

It should be noted that the impedance was computed with the liner geometry in place, due to the nature of the COMSOL Multiphysics® analytical model. Additionally, an option within the analytical model settings to include nonlinear effects was investigated. This model was compared with the others using the default nonlinear coefficients, but because the model relies on empirical parameters, it is not included in this report.

2.4 Simulation Test Cases

Three different experimental test cases were selected to compare with the COMSOL® simulations. Figure 6 illustrates each of these cases in two dimensions, but it should be noted that the thickness of each configuration is 0.25 in., with a total height of 1.00 in. and a width of 0.50 in.

The fins are at an angle of 45°, with the intrusion of the fins in A019 and A021 extending inward 0.125 and 0.187 in. from the outer walls, respectively. The expansion chamber fins on A024 are sloped to a -45° angle with each of the fins (starting from the top) extending to 0.066, 0.130, and 0.189 in. from the outer walls.

2.5 Simulation Results

The three comparison test cases are shown in Figure 7 to Figure 9.

As shown in Figure 7, the normalized resistance comparison is quite good for the bulk of the frequency spectrum for the A019 validation. The simulation lies right in the middle of the majority of the data points. The normalized reactance result is similar to the facesheet model comparison, where both the simulation and experiment flatten out and align near resonance. This produces an absorption coefficient comparison, with the simulation matching the experimental resonance peak very well.

As shown in Figure 8, the A021 predicted resistance lies on the majority of the experimental data points, similar to the A019 comparison. The predicted normalized reactance lines up with the experiment

at resonance, which produces an absorption coefficient peak aligning very well in location and magnitude, with this curve slightly narrower than in the A019 comparison.

Figure 9 compares expansion chamber concept A024 with the simulation. As with the previous two validation assessments, the normalized resistance comparison is unsurprising. The normalized reactance comparison is slightly better for this configuration. The absorption coefficient plot also yields a slight improvement compared with the previous two cases.

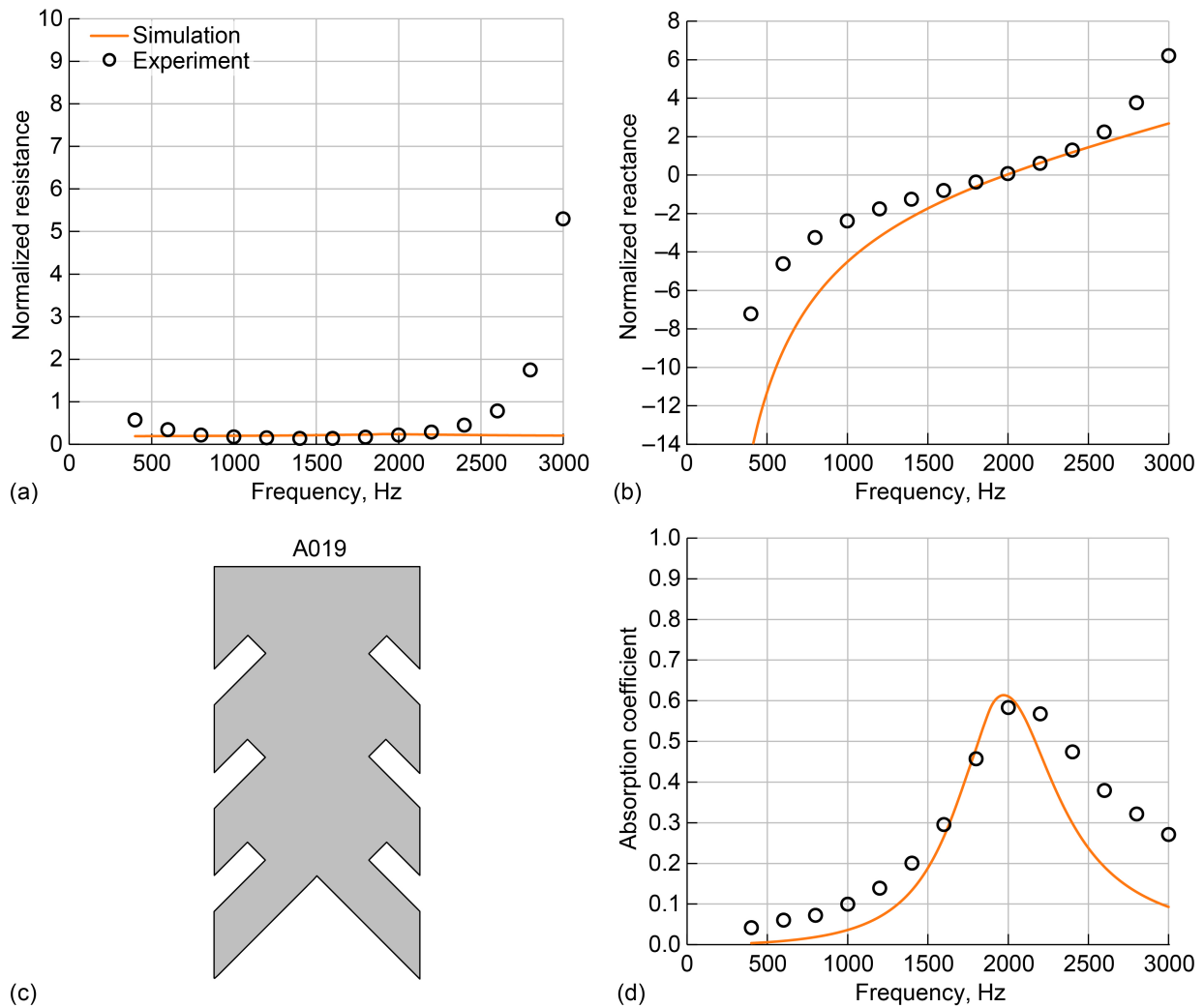


Figure 7.—Comparison of expansion chamber concept A019 with COMSOL Multiphysics® simulation. (a) Normalized resistance. (b) Normalized reactance. (c) Model. (d) Absorption coefficient.

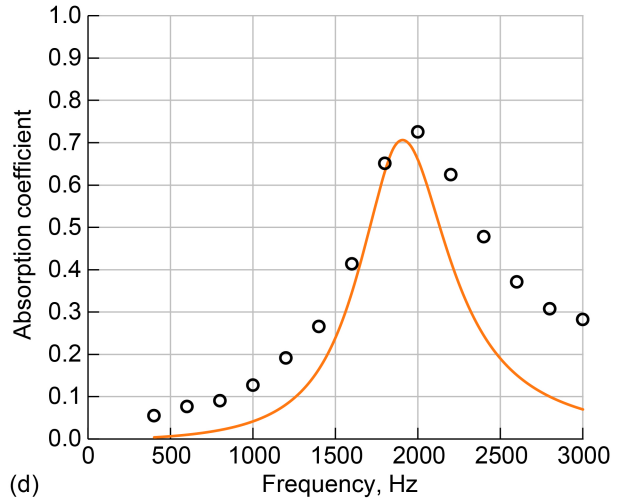
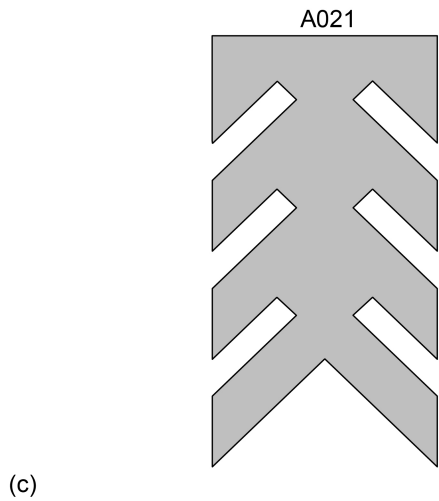
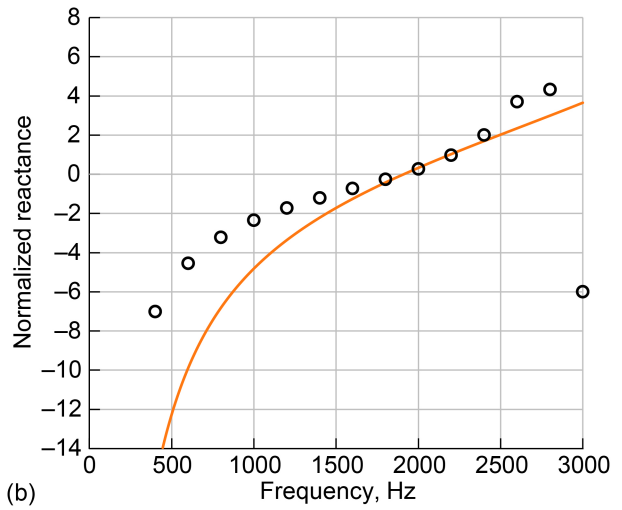
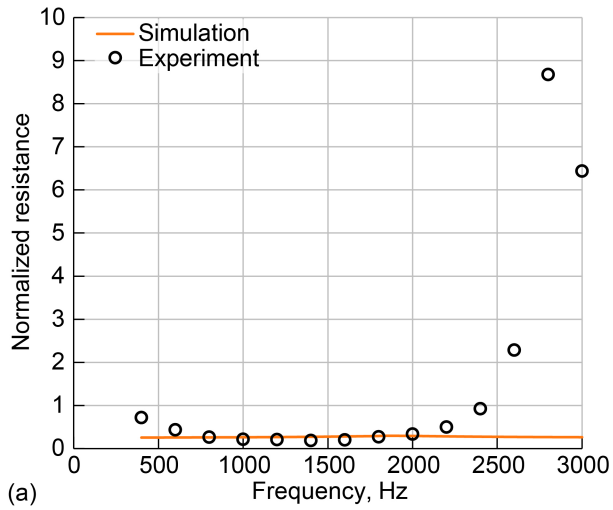


Figure 8.—Comparison of expansion chamber concept A021 with COMSOL Multiphysics® simulation. (a) Normalized resistance. (b) Normalized reactance. (c) Model. (d) Absorption coefficient.

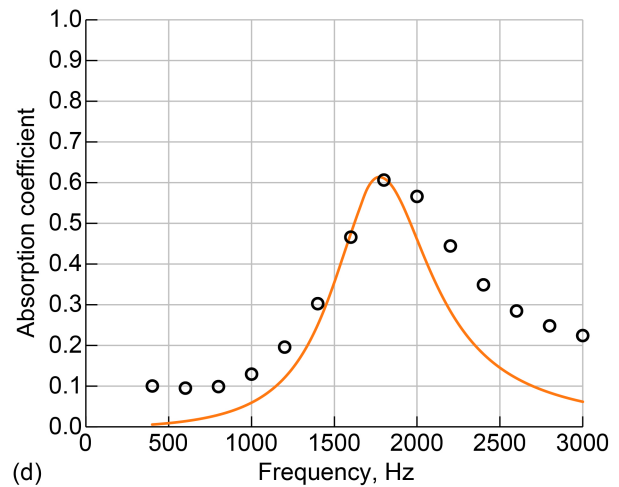
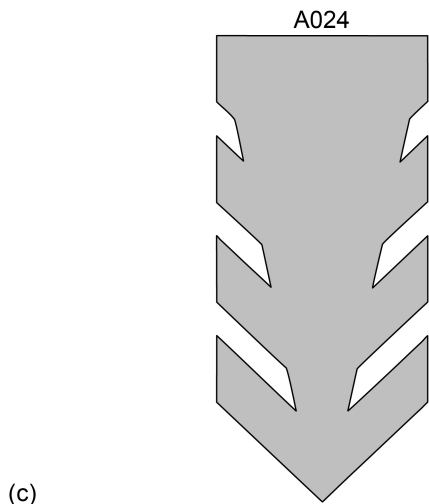
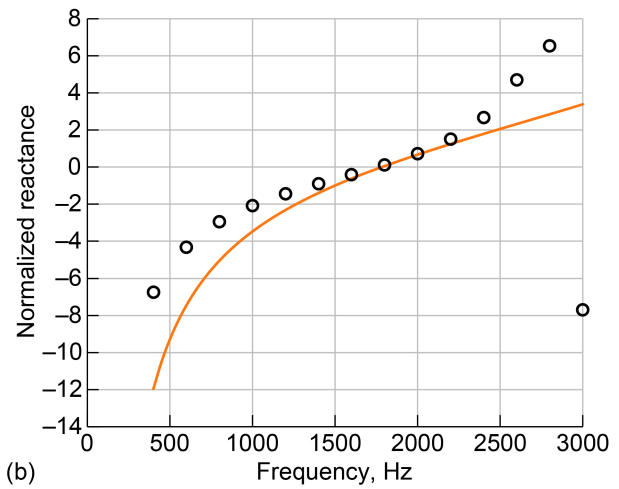
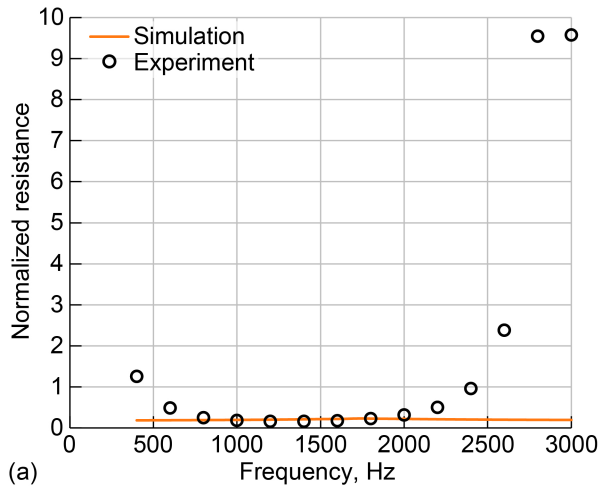


Figure 9.—Comparison of expansion chamber concept A024 with COMSOL Multiphysics® simulation. (a) Normalized resistance. (b) Normalized reactance. (c) Model. (d) Absorption coefficient.

2.6 Additional Test Cases Using Parametric Model

To better understand the acoustic mechanism at play for the expansion chamber design concepts, an additional parametric study was conducted on each of the design characteristics for these types of liners. By varying the expansion chamber fin length and angle, impedance and absorption coefficient predictions were made to analyze the acoustic response. Table I in the Appendix outlines the first part of the additional test cases run as part of this parametric study.

2.6.1 Parametric Results

For clarity, only plots for the absorption coefficient are presented in this report. The normalized surface impedance data are available upon request. Additionally, to reduce the number of data sets shown in each plot, only a subset of the results are presented. The rest are available upon request.

The first comparison plots, shown in Figure 10, are specifically comparing the effect of the expansion chamber fin angle; thus, the figure contains five different fin angles (-75° , -30° , 0° , 30° , 75°). It should also be noted that on both Figure 10 and Figure 11, the x-axis range of 400 to 3000 Hz has been truncated to 900 to 2400 Hz to better differentiate between data sets.

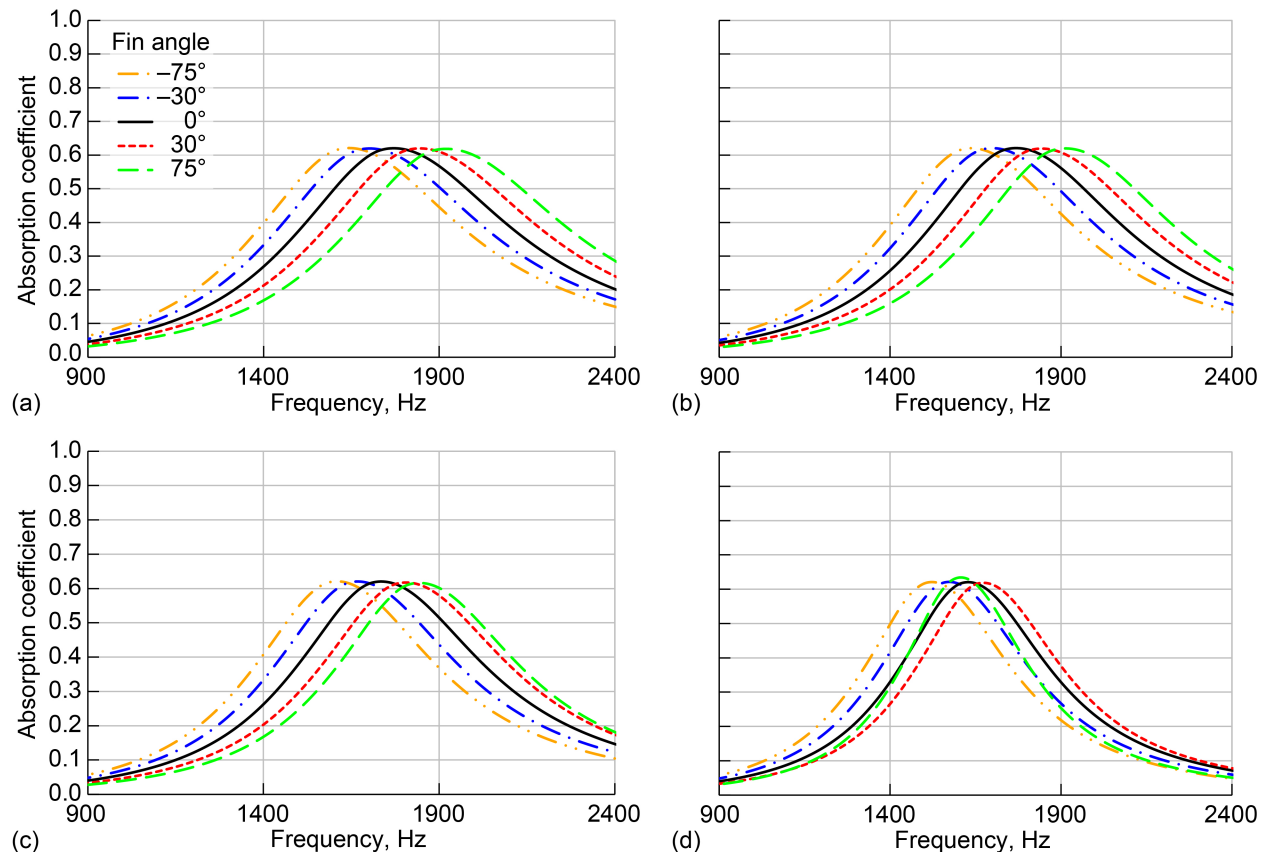


Figure 10.—Absorption coefficient comparison at various fin angles with constant fin length. (a) 0.05-in. fin. (b) 0.10-in. fin. (c) 0.15-in. fin. (d) 0.20-in. fin.

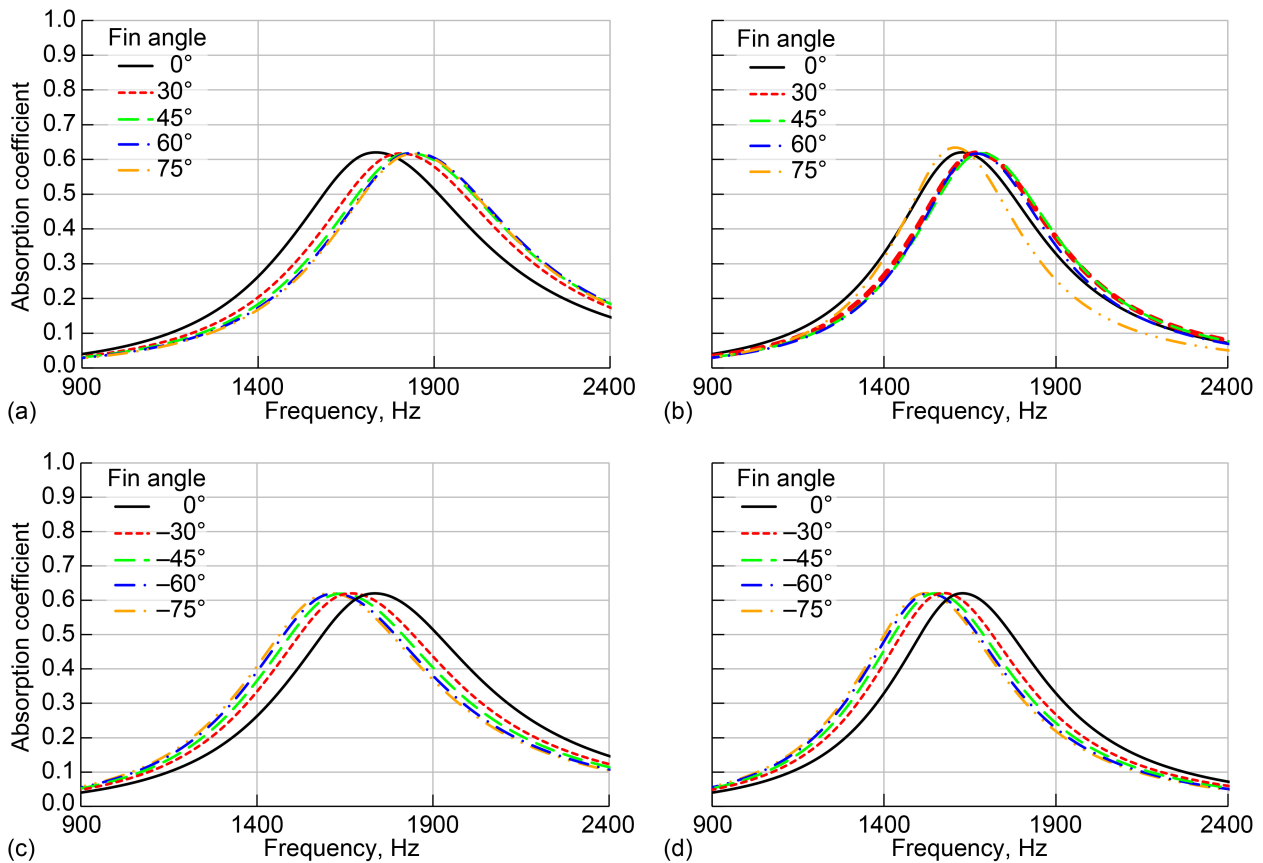


Figure 11.—Comparison fin angle orientation at constant fin length on absorption coefficient. (a) 0.15-in. positive fin angle. (b) 0.20-in. positive fin angle. (c) 0.15-in. negative fin angle. (d) 0.20-in. negative fin angle.

Although all four of the plots in Figure 10 look very similar, something interesting appears to occur when the fins become longer or closer together in the cavity. Generally, when the fins are positioned from the most negative angle and going toward the most positive angle, each of the data sets falls in line—with one exception. The case where the fins are in the 75° orientation and have a length of 0.2 in. results in one anomaly. In this case, it is suspected that the fins are just long enough and at an angle where the upper set is very close to the facesheet. This interaction appears to be what is disrupting the overall trend.

The next set of plots, shown in Figure 11, specifically investigates the fin angle orientation (positive or negative) and length. Because the previous plots showed little to no difference in results for cases where the fin lengths were 0.05 and 0.10 in., those results will be omitted from all further plots. They are available upon request. The following figure will begin from the case where the fin angle is horizontal and step up or down in angle increments (0°, 30°, 45°, 60°, 75°, 0°, -30°, -45°, -60°, -75°).

Upon closer investigation, it is evident that when comparing between positive and negative fin angle orientation, the design concepts with a negative orientation have a slightly lower resonance frequency. When the fins are in the positive orientation, the peak absorption shifts to the higher frequencies, albeit with the exception of the 75° case with fin lengths of 0.2 in. Overall, the majority of the data sets presented in Figure 11 appear to fall very close to one another depending on the orientation.

After producing and analyzing the impedance spectra and absorption coefficient plots corresponding with the test cases outlined in Table I in the Appendix, it appeared that the cases with the fins closer together yield a lower natural frequency. To dive deeper into the significance of the gap between the fins as well as many other design variables, the test cases outlined in Table II in the Appendix were analyzed. It should be noted that when the fins are close together, they could act as a thick perforate or possibly a slit.

To better visualize the difference between the angled backing cavity as well as the effect of an incrementally larger fin gap, design numbers 38, 39, and 40 are compared in Figure 12.

The peak resonance location for design 38 as compared with design 40 is slightly lower due to the slight reduction of the cavity length. Modification of the expansion chamber fin gap for each set of fins down the length of the cavity results in a slight increase in the absorption coefficient peak location. This indicates that the two lower sets of fins play a role in the liner's overall acoustic performance. It is clear, however, that the reduction of the fin gap distance does decrease the peak resonance location. Looking closer at designs 39 and 40, where the only difference is the backing cavity angle, a very slight increase in the resonance peak location is observed.

The effect of fin gap distance on the acoustic absorption characteristics was explored by further reduction in the fin gap, as shown in Figure 13.

Starting with design 50, which maintains a fin gap distance of 0.01 in., the absorption coefficient line begins to trail upward toward the end of the spectra. Based on the other two data sets present, there will likely be a second peak somewhere between 3000 and 3500 Hz. Reducing the fin gap further in designs 43 and 49 yields two absorption peaks, each of which is at a lower resonance frequency. The first absorption peak of design 43 is 200 Hz lower than that of design 50, and the first absorption peak of design 49 is 175 Hz lower than that of design 43.

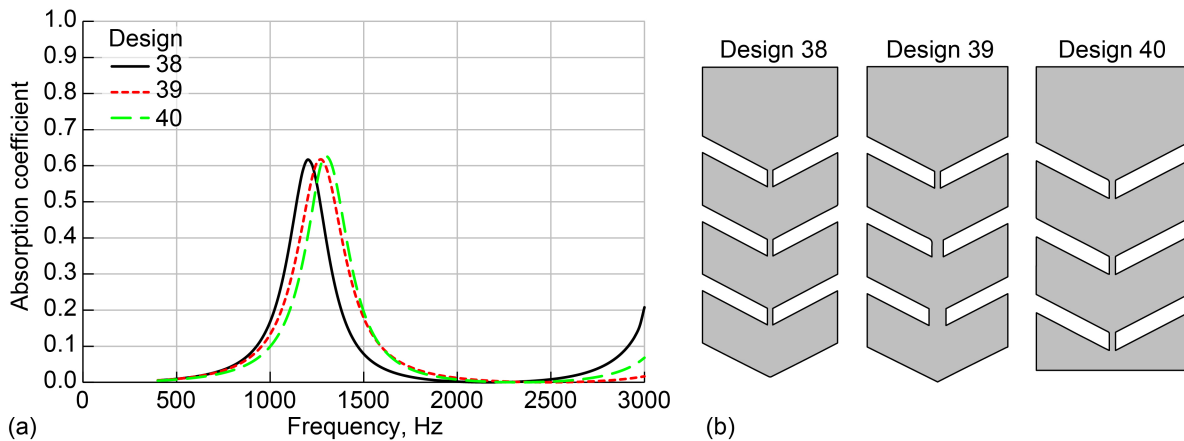


Figure 12.—Comparison of incrementally increasing fin gap distance (design 38 vs. 39) to constant fin gap, and comparison of angled backing cavity to flat backing cavity (design 38 vs. 40). (a) Absorption coefficient comparison. (b) Model.

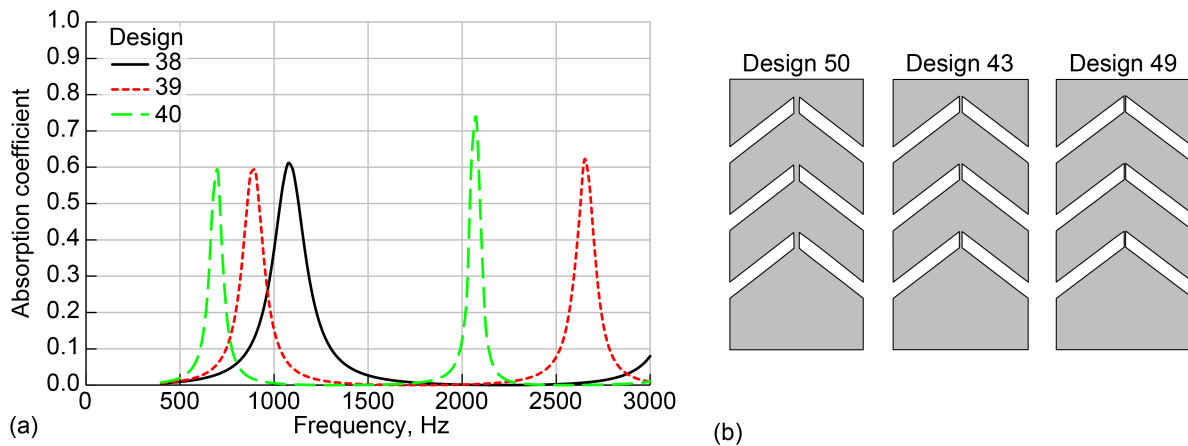


Figure 13.—Further comparison of absorption characteristics by reduction of fin gap distances. (a) Absorption coefficient comparison. (b) Model.

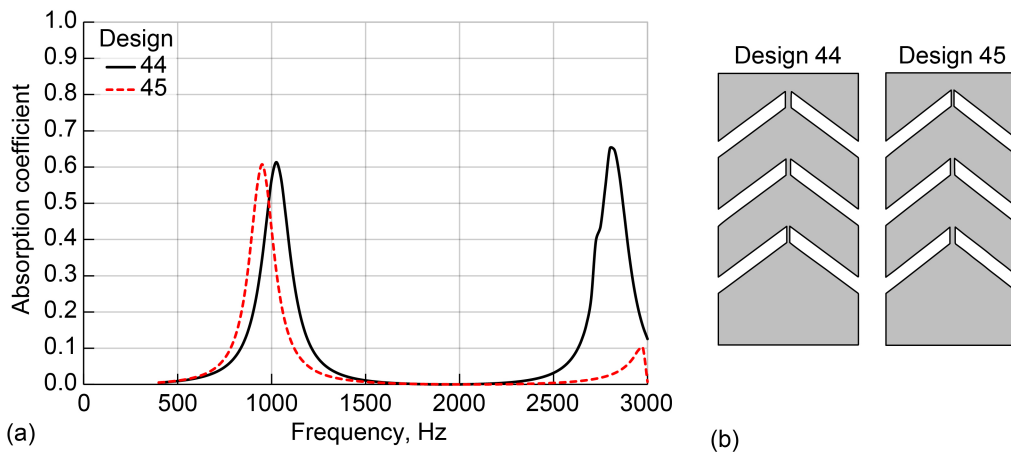


Figure 14.—Comparison of incrementally decreasing (design 44) or increasing (design 45) fin gap distance. (a) Absorption coefficient comparison. (b) Model.

Figure 14 compares designs 44 and 45 to look at an incremental decrease (design 44) and increase (design 45) in fin gap distance starting from the top of each design. The purpose of this comparison is to determine what effect, if any, the order in which the fin gap is incrementally increased or decreased has on the acoustic response.

Specifically isolating the comparison between designs 44 and 45, both contain the same fin gap distances of 0.01, 0.0075, and 0.005 in. Design 44 (which has the smallest gap on the bottom) yields two absorption peaks, whereas design 45 contains only one peak at a slightly lower resonance frequency than design 44.

Figure 15 presents test cases that have varying layers of expansion chamber fins. Starting with design 43 (which maintains a fin gap distance of 0.005 in.), one set of fins has been removed from the bottom, middle, and top of the cavity for test cases 46, 47, and 48, respectively.

Design 43 is used as the baseline for this comparison. Comparing design 46 with the baseline shows that by removing the bottom set of fins from the design, the second resonance peak is also removed from the acoustic response. Additionally, the first resonance peak increases by 25 Hz. Comparing design 47 with the baseline (where the middle set of fins are removed) shows that two absorption peaks are present, with the second peak yielding a much smaller band gap than the other design cases. Both peak resonance

locations are shifted to slightly higher frequencies. The first peak resonance location for design 47 increases by 100 Hz compared with that of design 46, and the first peak for design 48 is 100 Hz higher than that of design 47.

The final comparison in this series of test cases (Figure 16) removes another pair of expansion chamber fins. This comparison maintains a top fin gap of 0.005 in. with the two sets of fins beneath it removed, starting from the top and stepping down the single active fin location in each case. Leaving only one pair of expansion chamber fins results in a phenomenon similar to that discussed in the previous comparison. In this case, as the fins are relocated down the cavity, the absorption coefficient shifts to the higher frequencies. Comparing design 51 with design 43, the primary resonance frequency shifts by about 150 Hz. Stepping the fins down to compare design 52 with design 51, the absorption peak also increases about 150 Hz. The resonance peak for design 53 increases by 325 Hz as compared with design 52. Interestingly, design 53 also has a slightly increased band gap as well as two distinct absorption peaks.

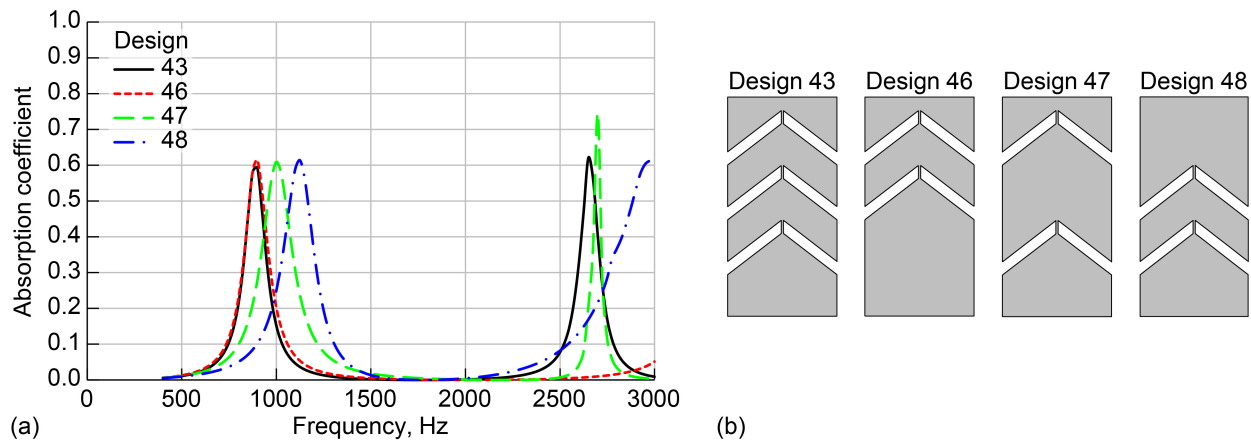


Figure 15.—Comparison of design cases with one set of fins removed to design case with all fins present with constant gap. (a) Absorption coefficient comparison. (b) Model.

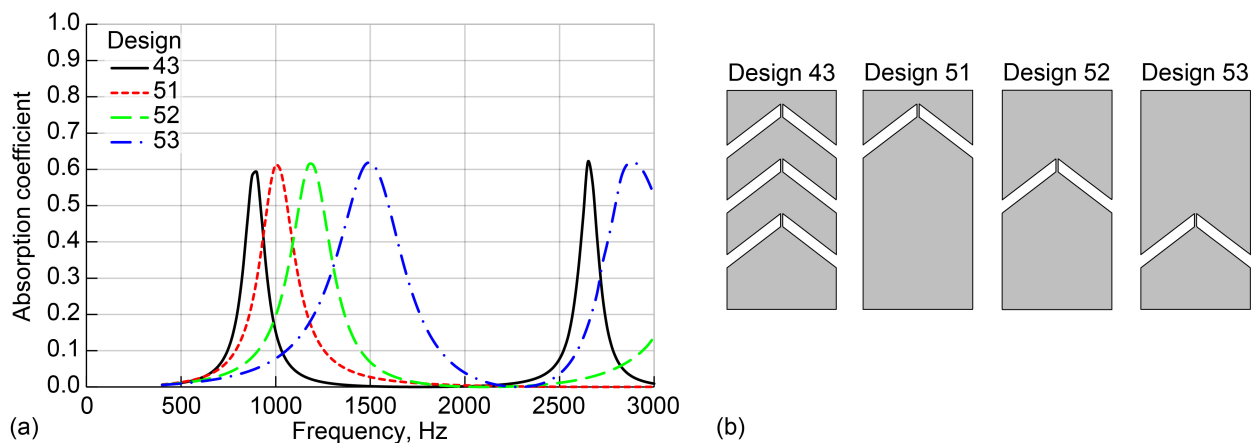


Figure 16.—Comparison of single set of fins with gap distance of 0.005 in. stepping down cavity. (a) Absorption coefficient comparison. (b) Model.

3.0 Conclusions

Four perforate models were investigated for use in modeling practices for over-the-rotor (OTR) expansion-chamber-type liner concepts. Of the four models, the two-parameter model was chosen as best suited for these concepts, which have nonstandard interior geometry. Converging on the particle velocity and the impedance within four runs yielded the best comparison. Comparing the COMSOL Multiphysics® (COMSOL AB) models for three different experimentally tested expansion chamber geometry concepts resulted in an accurate representation of the acoustic characteristics for this type of liner.

After evaluating some of the experimentally tested expansion chamber designs, a parametric model was constructed to better evaluate the active mechanism for optimal absorption. A series of 53 test cases were evaluated based on the initial design concepts where the expansion chamber fin length and angle were manipulated to better identify the acoustic characteristics. Fin lengths of less than 0.15 in. (for the current cavity geometry) had a minimal effect on the overall absorption coefficient peak and yielded almost identical results. When the expansion chamber fins were oriented in the negative direction, the resonance frequency peak was decreased by 100 Hz, and that peak was increased by 100 Hz when the fins were oriented in the positive direction. Additionally, changing the fin angle did not result in a significant acoustic trend in the absorption coefficient, but each of the data sets appeared to almost converge onto the others.

During the parametric study, the base design was modified to focus on the expansion chamber fin gap rather than the fin length. By reducing the fin gap, numerous resonance peaks were observed, albeit with a reduction in the resonance band gap. Removing one and eventually two of the three sets of expansion chamber fins shed some light on the culprit behind these multiple absorption peaks: numerous peaks appeared when there was a set of fins in the lowermost location. Design 47 shed further light on a design that contains a fairly low first resonance due to the top fins and which also contains a second peak due to the bottom fins.

Other design parameters are potentially worth investigating. Adding additional expansion chamber fins or varying the vertical fin spacing might have significant acoustic benefits. Varying the configuration within a liner sample—similar to a variable impedance liner aimed at broadband mitigation characteristics, but with a change in geometry rather than depth—is another possible approach; for example, 8 of the 15 cavities present could have one configuration and 7 could have another.

Appendix—Baseline and Design Configurations

Figure 1 from the Introduction is shown with a table describing the baseline parametric model expansion chamber test cases (Table I) and a table showing the targeted design configurations (Table II).

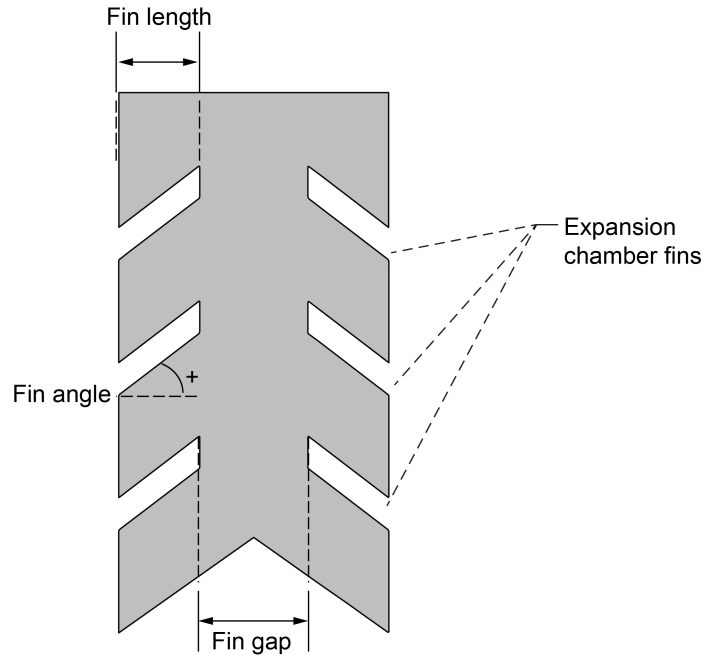


Figure 1.—Expansion chamber layout.

TABLE I.—BASELINE PARAMETRIC MODEL EXPANSION CHAMBER TEST CASES

Design number	Fin length, in.	Fin angle, deg	Design number	Fin length, in.	Fin angle, deg
1	0.00	0	20	0.15	75
2	0.05	0	21	0.20	75
3	0.10	0	22	0.05	-30
4	0.15	0	23	0.10	-30
5	0.20	0	24	0.15	-30
6	0.05	30	25	0.20	-30
7	0.10	30	26	0.05	-45
8	0.15	30	27	0.10	-45
9	0.20	30	28	0.15	-45
10	0.05	45	29	0.20	-45
11	0.10	45	30	0.05	-60
12	0.15	45	31	0.10	-60
13	0.20	45	32	0.15	-60
14	0.05	60	33	0.20	-60
15	0.10	60	34	0.05	-75
16	0.15	60	35	0.10	-75
17	0.20	60	36	0.15	-75
18	0.05	75	37	0.20	-75
19	0.10	75			

TABLE II.—ADDITIONAL SELECTED EXPANSION CHAMBER DESIGN TEST CASES

Design number	Top fin gap, in.	Middle fin gap, in.	Bottom fin gap, in.	Fin angle, deg	Backing cavity angle, deg
38	0.0100	0.0100	0.0100	-30	-30
39	0.0100	0.0200	0.0300	-30	-30
40	0.0100	0.0100	0.0100	-30	0
41	0.0050	0.0050	0.0050	-30	0
42	0.0050	0.0050	0.0050	30	0
43	0.0050	0.0050	0.0050	45	0
44	0.0100	0.0075	0.0050	45	0
45	0.0050	0.0075	0.0100	45	0
46	0.0050	0.0050	No bottom fin	45	0
47	0.0050	No middle fin	0.0050	45	0
48	No top fin	0.0050	0.0050	45	0
49	0.0025	0.0025	0.0025	45	0
50	0.0100	0.0100	0.0100	45	0
51	0.0050	No middle fin	No bottom fin	45	0
52	No top fin	0.0050	No bottom fin	45	0
53	No top fin	No middle fin	0.0050	45	0

References

1. Parrott, Tony L.; and Jones, Michael G.: Parallel-Element Liner Impedances for Improved Absorption of Broadband Sound in Ducts. *Noise Control Eng. J.*, vol. 43, no. 6, 1995.
2. Jones, M.G.; Howerton, B.M.; and Ayle, E.: Evaluation of Parallel-Element, Variable-Impedance, Broadband Acoustic Liner Concepts. AIAA 2012–2194, 2012.
3. Jones, Michael G.: An Over-the-Rotor Liner Investigation With Configurations Enabled by Additive Manufacturing. NASA/TM-20205010863, 2020. <https://ntrs.nasa.gov>
4. Bozak, Richard F.; and Podboy, Gary G.: Evaluating the Aerodynamic Impact of Circumferentially Grooved Fan Casing Treatments With Integrated Acoustic Liners on a Turbofan Rotor. ASME GT2019–91369, 2019.
5. Sutliff, Daniel L.; and Jones, Michael G.: Low-Speed Fan Noise Attenuation From a Foam-Metal Liner. *J. Aircr.*, vol. 46, no. 4, 2009, pp. 1381–1394.
6. Jones, Michael G., et al.: Over-the-Rotor Liner Investigation via the NASA Langley Normal Incidence Tube. NASA/TM–2019-22043, 2019. <https://ntrs.nasa.gov>
7. Elliott, David M.; Woodward, Richard P.; and Podboy, Gary G.: Acoustic Performance of Novel Fan Noise Reduction Technologies for a High Bypass Model Turbofan at Simulated Flight Conditions. AIAA 2009–3140, 2009.
8. Jones, M.G., et al.: Assessment of Soft Vane and Metal Foam Engine Noise Reduction Concepts. AIAA 2009–3142, 2009.
9. Sutliff, Daniel L.; Jones, Michael G.; and Hartley, Thomas C.: High-Speed Turbofan Noise Reduction Using Foam-Metal Liner Over-the-Rotor. *J. Aircr.*, vol. 50, no. 5, 2013, pp. 1491–1503.
10. Elliott, D.M.: Over the Rotor and Soft Vanes on the Source Diagnostic Test Model in the NASA Glenn 9×15 Low-Speed Wind Tunnel. To be published as a NASA Technical Memorandum.
11. Jones, M.G.; and Howerton, B.M.: Evaluation of Novel Liner Concepts for Fan and Airframe Noise Reduction. AIAA 2016–2787, 2016.
12. Gazella, Matthew R., et al.: Evaluating the Acoustic Benefits of Over-the-Rotor Acoustic Treatments Installed on Advanced Noise Control Fan. AIAA 2017–3872, 2017.
13. Bozak, Richard F.; and Dougherty, Robert P.: Measurement of Noise Reduction From Acoustic Casing Treatments Installed Over a Subscale High Bypass Ratio Turbofan Rotor. AIAA 2018–4099, 2013.
14. Bozak, Richard F., et al.: Effect of Grazing Flow on Grooved Over-the-Rotor Acoustic Casing Treatments. AIAA 2019–2564, 2019.
15. Palleja-Cabre, Sergi, et al.: Modelling of Over-the-Rotor Acoustic Treatments for Improved Noise Suppression in Turbofan Engines. AIAA 2017–2580, 2017.
16. Sutliff, Daniel L., et al.: Investigations of Three Over-the-Rotor Liner Concepts at Various Technology Readiness Levels. *Int. J. Aeroacoustics*, vol. 20, nos. 5–7, 2021, pp. 826–866.
17. COMSOL: COMSOL Multiphysics Programming Reference Manual. Version 5.6, 2020.
18. Chung, J.Y.; and Blaser, D.A.: Transfer Function Method of Measuring In-Duct Acoustic Properties: I. Theory. *J. Acoust. Soc. Am.*, vol. 68, 1980, pp. 907–921.
19. Jones, Michael G.; and Parrott, Tony L.: Evaluation of a Multi-Point Method for Determining Acoustic Impedance. *MSSP*, vol. 3, no. 1, 1989, pp. 15–35.
20. Hubbard, Harvey H., ed.: Design and Performance of Duct Acoustic Treatment. *Aeroacoustics of Flight Vehicles: Theory and Practice*, NASA Reference Publication 1258, Vol. 2: Noise Control, Ch. 14, 1991. <https://ntrs.nasa.gov>

21. Dahl, Milo D., ed.: Assessment of NASA's Aircraft Noise Prediction Capability. Chapter 6—Uncertainty in Acoustic Liner Impedance Measurement and Prediction, NASA/TP—2012-215653, 2012. <https://ntrs.nasa.gov>
22. Jones, Michael G., et al.: A Review of Acoustic Liner Experimental Characterization at NASA Langley. NASA/TP—2020-220583, 2020. <https://ntrs.nasa.gov>
23. Jones, M.G.; and Watson, W.R.: On the Use of Experimental Methods to Improve Confidence in the Educated Impedance. AIAA 2011–2865, 2011.

